International Journal of Nanomedicine

Dovepress
open access to scientific and medical research

Open Access Full Text Article

ORIGINAL RESEARCH

Empowering Cartilage Restructuring with Biodegradable Magnesium Doped-Silicon Based-Nanoplatforms: Sustained Delivery and Enhanced Differentiation Potential

Min Chen[1,*], Tao Liu[2,*], Wenqiang Li[3], Yingting Li[1], Puxin Zhong[1], Huanchen Yan[1], Jingyin Kong[1], Weixiang Liang[2]

[1]Department of Obstetrics and Gynecology, Department of Fetal Medicine and Prenatal Diagnosis; Guangdong Provincial Key Laboratory of Major Obstetric Diseases; Guangdong Provincial Clinical Research Center for Obstetrics and Gynecology; Guangdong-Hong Kong-Macao Greater Bay Area Higher Education Joint Laboratory of Maternal-Fetal Medicine; The Third Affiliated Hospital of Guangzhou Medical University, Guangzhou, 510000, People's Republic of China; [2]Department of Ultrasound; Guangdong Provincial Key Laboratory of Major Obstetric Diseases; Guangdong Provincial Clinical Research Center for Obstetrics and Gynecology; The Third Affiliated Hospital of Guangzhou Medical University, Guangzhou, 510000, People's Republic of China; [3]Engineering Technology Research Center for Sports Assistive Devices of Guangdong, Guangzhou Sport University, Guangzhou, 510076, People's Republic of China

*These authors contributed equally to this work

Correspondence: Min Chen, Email edchen99@gmail.com

Background: Cartilage-related diseases, such as hypoplastic chondrodysplasia a rare genetic disorder that affects newborns, causing abnormal cartilage development and restricted skeletal growth. However, the development of effective treatment strategies for chondrodysplasia still faces significant challenges due to limitations in the controlled drug delivery, biocompatibility, and biodegradability of nanomedicines.

Methods: A biodegradable magnesium doped-silicon based-nanoplatforms based on silicon nanoparticles (MON) was constructed. Briefly, the MON was modified with sulfhydryl groups using MPTMS to form MOS. Further engineering of MOS was achieved by incorporating Mg^{2+} ions through the "dissolution-regrowth" method, resulting in MMOS. Ica was effectively loaded into the MMOS channels, and HA was anchored on the surface of MOS to obtain MMOS-Ica@HA nanoplatforms. Additionally, in vitro cell experiments and in vivo zebrafish embryo models were used to evaluate the effect of the nanoplatforms on cartilage differentiation or formation and the efficiency of treating chondrodysplasia.

Results: A series of characterization tests including TEM, SEM, DLS, XPS, EDX, and BET analysis validate the successful preparation of MOS-Ica@HA nanoplatforms. The prepared nanoplatforms show excellent dispersion and controllable drug release behavior. The cytotoxicity evaluation reveals the good biocompatibility of MOS-Ica@HA due to the sustained and controllable release of Ica. Importantly, the presence of Ica and Mg component in MOS-Ica@HA significantly promote chondrogenic differentiation of BMSCs via the Smad5/HIF-1α signaling pathway. In vitro and in vivo experiments confirmed that the nanoplatforms improved chondrodysplasia by promoting cartilage differentiation and formation.

Conclusion: The findings suggest the potential application of the developed biodegradable MMOS-Ica@HA nanoplatforms with acceptable drug loading capacity and controlled drug release in chondrodysplasia treatment, which indicates a promising approach for the treatment of chondrodysplasia.

Keywords: nanoplatforms, controlled release, biocompatibility, chondrodysplasia, cartilage differentiation

Introduction

Chondrodysplasia is a rare and complex genetic disorder that affects newborns, leading to abnormal development of cartilage tissue and restricted skeletal growth.[1–5] It evidently imposes severe physical and functional impairments on

Received: 8 November 2023
Accepted: 8 January 2024
Published: 17 January 2024

affected infants, greatly impacting their quality of life and future development. Consequently, research on cartilage-related diseases, including chondrodysplasia in newborns has garnered increasing attention within the scientific community.[6,7]

In recent decades, significant progress has been made in the study of cartilage dysplasia. Ongoing approaches, including gene therapy, cell therapy, and drug interventions, show promise in promoting the differentiation and growth of cartilage cells,[8–11] thereby improving skeletal development in affected individuals. For instance, a study by Liu et al[12] highlighted the potential of Icariin (Ica), a flavonoid compound extracted from the Epimedium herb, to promote chondrogenesis in mesenchymal stem cells (MSCs) when exposed to a conditioned medium. Ica has also been shown to support chondrocyte proliferation, maintain their distinct phenotype, enhance the secretion of proteoglycan and collagen matrix, and prevent collagen and proteoglycan efficacy in treating chondrodysplasia disorders.[13–15] Additionally, Ica has been reported to have anti-inflammatory effects, which can inhibit the production of inflammatory mediators and the activation of inflammatory signaling pathways in addition to treating chondrodysplasia by promoting chondrocyte proliferation and differentiation, thereby attenuating the adverse effects of the inflammatory response on chondrogenesis.[16–18] However, sustained administration or high doses of Ica may inhibit chondrocyte proliferation and potentially pose unnecessary biosafety risks to a certain extent.[19] Therefore, there is an urgent need to design biodegradable nano-drug carriers with favorable drug availability and controllable release for effective delivery of Ica and other therapeutic agents in the treatment of these disorders.

As one of the well-known drug delivery systems (DDSs), mesoporous organic silicon nanoparticles (MON) are widely used in various biomedical fields due to their unique porous structure, good biocompatibility, and biodegradability.[20–24] Especially, further engineering of MON frameworks with metallic ions (eg, -Si-O-M-, where M = Fe, Cu, Mg, Ca) can endow the MON system with additional biological properties.[25] For example, Huang et al[26] reported a silver engineered-silica nanoparticles to accelerate chronic wound healing by regulating inflammatory response and inhibiting bacteria. Wang et al[27] developed iron-engineered mesoporous silica nanocatalyst for specific anti-tumor therapy based on enhanced Fenton-like reactions. Therefore, the strategies of metal-engineered silica nanoparticles can endow them with multifunctionality.

Magnesium is a vital micronutrient necessary for proper bodily functions and has established a growing connection between Mg^{2+} deficiency and orthopedic ailments like cartilage defect and osteoporosis.[28,29] Notably, studies have demonstrated that Mg^{2+} plays a crucial role in promoting the adhesion and chondrogenesis of synovial mesenchymal stem cells (SMSCs) through integrins.[30,31] Additionally, Mg^{2+} has been found to inhibit extracellular matrix (ECM) calcification and safeguard articular cartilage by activating the HIF-1α to improve chondrogenesis pathway.[32,33] It can be reasonably speculated that Mg-engineered MON has prominent application prospects in promoting cartilage reconstruction. However, the integration of metal ions and silica nanoparticles in engineering processes often leads to nanoparticle aggregation and uncontrollable structural damage.[34] These challenges pose significant obstacles to the use of metal-engineered silica nanoparticles in future biomedical applications.

To overcome the above concerns, we pioneeringly constructed a biodegradable magnesium doped-silicon based-nanoplatforms for optimizing drug delivery and efficiently treating chondrodysplasia. In brief, the MON is decorated with sulfhydryl groups through the grafting of 3-mercaptopropyltrimethoxysilane (MPTMS), resulting in the formation of MOS, and the MOS is further engineering with Mg^{2+} via the "dissolution-regrowth" method to obtain MMOS. Due to its unique structure, Ica is effectively loaded into the MMOS channel and achieves appreciable drug-loading capacity. After that, hyaluronic acid (HA) as a gate is anchored on the surface of MOS to construct MMOS-Ica@HA (Scheme 1a). A series of measurements and characterizations, such as TEM observation, particle size distribution, EDX, XPS, and BET analysis were conducted to verify the successful preparation of MMOS-Ica@HA. The cytotoxicity of MMOS-Ica @HA was comprehensively evaluated by cell proliferation assay, live-dead staining, or cell morphology and spreading after staining of the cytoskeleton. Furthermore, the effect of nanoplatforms on cartilage differentiation and formation was examined through in vitro cell culture and in vivo zebrafish embryo models with chondrodysplasia, validating that the MOS-Ica@HA can improve the chondrodysplasia by promoting the differentiation and formation of cartilage (Scheme 1b).

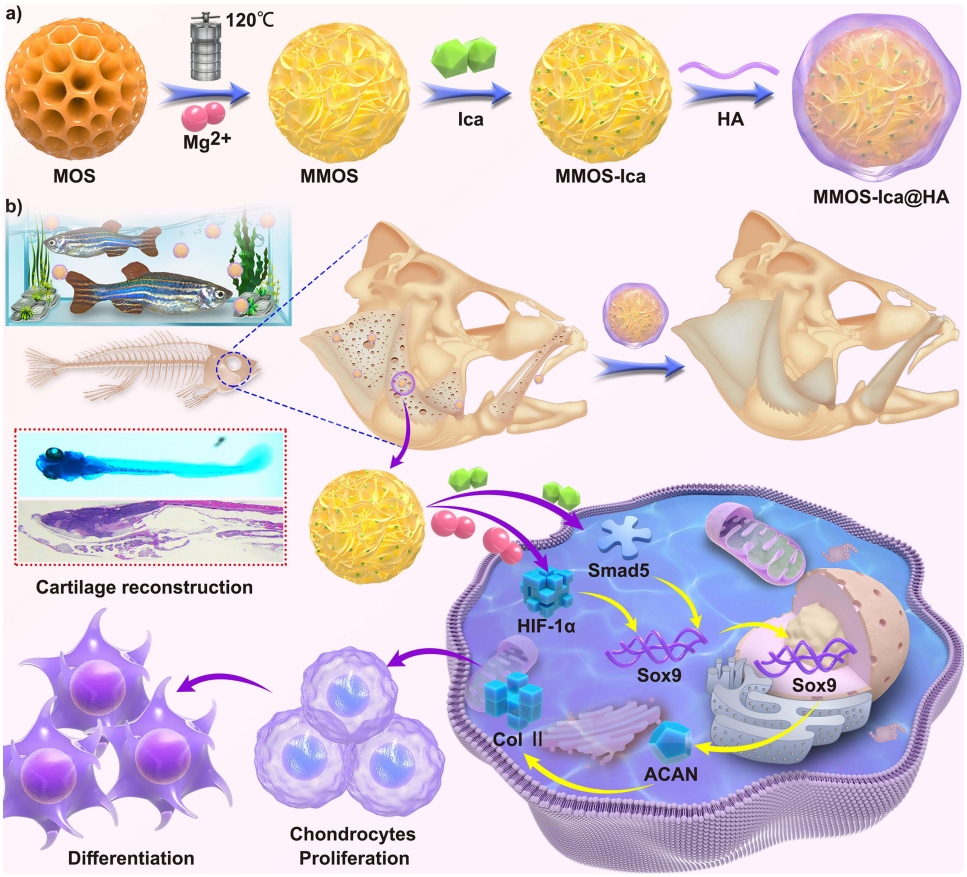

Scheme 1 (**a**) Construction of MOS-Ica@HA nanocapsules. (**b**) Schematic illustration of MOS-Ica@HA nanocapsules for treatment of zebrafish chondrodysplasia by promoting the proliferation and differentiation of chondrocytes.

Experimental Section

Materials

Tetraethyl orthosilicate (TEOS) and triethanolamine (TEA) were bought from Aladdin Reagent (China). Cetanecyltrimethylammonium chloride (CTAC), bis (3-triethoxysilylproyl) disulfide (BTDS) was purchased from Shanghai Yuanye Biological Technology Co., Ltd. Magnesium chloride hexahydrate ($MgCl_2{\cdot}6H_2O$), hyaluronic acid (HA, sodium salt, M_w = 500–600 kDa, 99%), and dexamethasone was provided from Sigma-Aldrich (USA). Ammonium chloride (NH_4Cl), ammonium hydroxide ($NH_3{\cdot}H_2O$, 28%) glutathione (GSH, 98.0%), rhodamine6G (R6G), and MPTMS were purchased from Shanghai Macklin Biochemical Co., Ltd. Primary antibodies of anti-collagen type II (COL II), anti-aggrecan (ACAN), sex-determining region Y-box 9 (SOX 9) were provided from Abcam and Life Technology. All chemical reagents were analytical grade.

Synthesis of MON and MOS

Typically, the procedure involves stirring a mixture of 20 g CTAC (10 wt%) and 0.8 g TEA aqueous solution (10 wt%) at 90 °C for 30 minutes. Subsequently, 1.0 mL of TEOS is added. After 1 h, a mixture of 1 mL TEOS and 0.6 mL BTDS, serving as mixed silicon sources, is introduced with stirring for 4 h. The resulting product is a white precipitate (eg, MON), which is obtained through centrifugation and subsequent washing steps. For the synthesis of MOS, 100 mg of MOS was dispersed in 100 mL of isopropanol. Subsequently, 200 μL of MPTMS was added to the mixture, and the solution was refluxed at 80 °C overnight. The MOS precipitates were acquired by centrifugation and washing procedures.

Synthesis of MMOS

100 mg of MOS was dispersed in 10 mL of an aqueous solution and combined with 2 mL of a $MgCl_2$ solution (15.6 mg/mL) under magnetic stirring for 45 minutes. Following this, 0.436 g of NH_4Cl and 1.0 mL of $NH_3{\cdot}H_2O$ (28%) were added to the mixture. After stirring for 2.0 h, the solution was transferred to a Teflon-lined autoclave and maintained at 120 °C for 18 h. The resulting MMOS was obtained by centrifugation at 20,000 ×g for 15 min, followed by washing with pure water five times. Finally, the product was freeze-dried under a vacuum condition.

Synthesis of MMOS-Ica@HA

To initiate the Ica loading process, a dispersion of MMOS (4.0 mL, 2.5 mg/mL) was mixed with 1.0 mL of Ica solution (2.0 mg/mL) and stirred overnight at room temperature. The resulting solution was then subjected to centrifugation (20,000 × g, 10 minutes) and washed to obtain MMOS-Ica. Subsequently, HA was used for surface modification and block. The MMOS-Ica obtained previously was dissolved in a HA solution (5.0 mL, 0.5 mg/mL) and stirred for 12 h. Afterward, the solution was centrifuged (20,000 × g, 10 min) and rinsed twice with MilliQ water to obtain MMOS-Ica @HA. The supernatants from each step were collected for UV-vis analysis at a wavelength of 360 nm to determine the Ica loading content.

The morphology and distribution of the MMOS and MMOS-Ica@HA nanoparticles were assessed using transmission electron microscopy (TEM) with a Philips CM-120 instrument from Eindhoven, Netherlands. Additionally, TEM measurements provided elemental mappings and energy-dispersive X-ray spectroscopy (EDS) spectra for the AMSN nanoparticles. The composition of MMOS-Ica@HA was analyzed by X-ray photoelectron spectroscopy (XPS) spectrum.

Assessment of Biodegradability Behavior

To investigate the degradation behavior of the nanoplatforms, MOS, MMOS, and MMOS-Ica@HA (20 μL, 10 mg/mL) were incubated with 1.0 mL of simulated body fluid (SBF) solution containing 1.0 mM GSH at 37 °C with shaking. After incubating for 1, 3, 5, or 7 days, a 10 μL portion of the solution was extracted for TEM measurement to observe the degradation behavior of the nanoplatforms.

In vitro Drug Release

2.0 mL aqueous solution of MMOS-Ica or MMOS-Ica@HA (1.0 mg/mL) was enclosed in a dialysis bag with a molecular weight cutoff of 3.5 kDa. The dialysis bag was then immersed in 10 mL of PBS containing either 0.5 or 1.0 mM GSH. The dialysis process was carried out at 37 °C in a culture incubator with gentle shaking at 100 rpm. At specific time intervals of 0.25, 0.5, 1.0, 2.0, 3.0, 5.0, or 7.0 days, 0.5 mL of the PBS solution was taken out and replaced with fresh PBS of the same conditions and volume. The released Ica in the PBS was quantified using a UV-vis spectrophotometer, while the released Mg^{2+} ions were measured using inductively coupled plasma optical emission spectrometry (ICP-OES) with a Thermo Fisher Scientific iCAP 6300Duo instrument.

R6G-Labeled Nanoplatforms

To label nanoplatforms with R6G, a dispersion of nanoplatforms (10 mL, 1.0 mg/mL) was mixed with R6G (100 μL, 15 mg/mL) and stirred in the dark for 24 h. The resulting R6G-labeled MOS, MMOS, or MMOS-Ica@HA was obtained by centrifugation at 15,000 × g for 10 minutes, followed by washing with deionized water for subsequent use.

In vitro Cell Analysis

Cell Isolation and Culture

SD rats (4 days old, provided by Guangdong Provincial Animal Experiment Center) were used to obtain bone marrow mesenchymal stem cells (BMSCs). The rats were anesthetized with pentobarbital sodium and sterilized by soaking in 75% absolute ethanol. The femoral marrow cavities were then accessed to collect the bone marrow extracts. These extracts were cultured in a complete culture medium consisting of α-MEM, 1% PS, and 10% FBS. The initial BMSCs were purified at passages 3–4 to be used for further studies.

Endocytosis Performance of R6G-Labeled Nanoplatforms

BMSCs were seeded into confocal dishes at a density of 5.0×10^4 cells and allowed to adhere overnight. The growth media were then replaced with 0.5 mL of culture medium containing R6G-labeled MOS, MMOS, or MMOS-Ica@HA at a concentration of 4.0 μg/mL for R6G. The cells were incubated for an additional 2.0 h. Subsequently, the treated cells were washed with PBS and fixed using a 4.0% paraformaldehyde solution. To visualize the cell nuclei, DAPI staining was performed for 15 min. The obtained cells were followed by treatment with a Rhodamine-Phalloidin solution containing 0.1% Triton X-100 and 1.0% BSA for 20 min. Finally, the cells were observed using laser scanning confocal microscopy (LSCM).

To prepare for flow cytometry analysis, BMSCs were seeded into 6-well plates at a density of 2.0×10^5 cells per well and allowed to adhere overnight. Subsequently, the culture medium was replaced with the fresh culturing medium. (1.0 mL) containing R6G-labeled MMOS-Ica@HA (C_{R6G} = 4.0 μg/mL). After an additional 2.0 h of incubation, the cells were washed twice with cold PBS and harvested by trypsinization. The cell suspension was then centrifuged at 2000 × g for 3.0 min. The resulting cell pellet was re-suspended in PBS and subjected to analysis using flow cytometry. (Guava easyCyte, USA).

Cytotoxicity Assay

To evaluate the cytocompatibility of various formulations, an MTT assay was conducted. BMSCs were seeded into 96-well plates at a density of 5.0×10^3 cells per well and incubated overnight at 37 °C. Subsequently, the culture medium was replaced with fresh complete culture medium containing different concentrations (ranging from 0 to 400 μg/mL) of PBS, MOS, MMOS, MMOS-Ica, and MMOS-Ica@HA. After co-incubation for 1.0, 3.0, and 5.0 days, the relative cell viability was assessed using a standardized method. Meanwhile, BMSCs treated with MOS, MMOS, MMOS-Ica, and MMOS-Ica@HA at a concentration of 100 μg/mL for 3.0 days were subjected to a live/dead assay.

Furthermore, the cell morphology and spreading ability of BMSCs were assessed after co-incubation with different nanoplatforms. Subsequently, the collected cell samples were fixed in 4% paraformaldehyde, permeabilized with 0.1% Triton X-100, blocked with bovine serum albumin, and then subjected to immunostaining using Rhodamine-Phalloidin for F-actin filaments and DAPI for the nucleus in a dark environment. The samples were then observed using LSCM. As for the quantitative analysis of live/dead cells or cell spreading area, which was determined by the regions of the three replicates by Image J software.

BMSCs Chondrogenic Differentiation Assay

BMSCs were cultured in 15 mL centrifuge tubes using the chondrogenic medium. The medium was refreshed every 2 days with fresh medium and a solution containing nanoplatforms (10 μL) for a period of 14 days. Following the incubation, the resulting cell pellets were frozen and sliced into sections with a thickness of 5 μm. These sections were then subjected to Alcian blue and Safranin-O staining. Additionally, BMSCs were cultured for 14 days in a chondrogenic medium supplemented with the nanoplatform solution. To assess the expression of cartilage-related markers (including Col-II, ACAN, SOX9), quantitative real-time PCR (qPCR) analysis was performed. The gene sequences of Col-II, ACAN, and SOX9 are described in Table 1.

Besides, to visualize the expression of cartilage-related proteins, immunofluorescence staining was employed. Primary antibodies targeting Col-II, or SOX9 were utilized, followed by incubation with goat anti-mouse IgG secondary antibodies labeled with Alexa Fluor®594 or Alexa Fluor®488. To visualize the cell nuclei, DAPI was used as a counterstain. The resulting images were captured using a fluorescence microscope.

In vivo Cartilage Regeneration Assessment

Construction of a Model of Embryonic Chondrodysplasia in Zebrafish

The adult wild-type zebrafish (AB, bought from the Animal Experiment Center of Southern Medical University) used in this study were obtained from the Zebrafish Research Centre of Southern Medical University, China. The zebrafish were housed individually in a water purification system provided by Shanghai Aquarium Devices Company, China. To initiate the breeding process, the zebrafish were transferred to a mating pool with a sex ratio of 1:2 (male to female). Spawning

Table 1 The Sequence of Primers

Gene Name	Sequence	
GAPDH	F	TCACCATCTTCCAGGAGCGA
	R	CACAATGCCGAAGTGGTCGT
Col-II	F	AAGAGCGGTGACTACTGGATAG
	R	TGCTGTCTCCATAGCTGAAGT
ACAN	F	AGGTCGTGGTGAAAGGTGTTG
	R	GTAGGTTCTCACGCCAGGGA
Sox9	F	GGTGCTCAAGGGCTACGACT
	R	GGGTGGTCTTTCTTGTGCTG

was induced in the morning when the lights were turned on, simulating natural conditions. After approximately 30 min, the embryos were collected in a dish. These embryos were then placed in egg water, which is a culture medium containing 5–10% methylene blue (Sigma). After the embryo developed to 2 days post-fertilization (dpf), the zebrafish embryo was treated with prednisolone (10 μM) to construct the model of zebrafish with chondrodysplasia. All animal procedures were performed in accordance with the Guidelines for Care and Use of Laboratory Animals of Guangzhou Medical University and approved by the Animal Ethics Committee of Guangzhou Medical University. The assigned approval/accreditation number is SYXK(YUE)2023-0112.

Pharmacological Treatment

The obtained zebrafish chondrodysplasia model was divided randomly into four groups: PBS (control group), MOS (2.0 mg/mL), MMOS (2.0 mg/mL), and MMOS-Ica@HA (2.0 mg/mL) groups. Subsequently, the embryos in each group were exposed to the pharmacological drug MMOS-Ica@HA from 3 to 7 dpf. At 7 dpf, the larvae from all groups were subjected to an assay to evaluate the development of their craniofacial cartilage structures.

Cartilage Reconstruction Ability in the Zebrafish Embryo

At the end of 7 dpf, the larvae from different groups, including those treated with nanoplatforms and the control group were thoroughly washed and then euthanized using a lethal dose of MS-222. Following euthanization, the larvae were fixed in a solution consisting of 4% paraformaldehyde (PFA) in phosphate-buffered saline (PBS). For visualization of the cartilage development in zebrafish, the prepared slices were subjected to staining techniques. Two staining methods, namely alcian blue, and hematoxylin-eosin (H&E), were employed. Alcian blue staining specifically highlights the presence of cartilage by binding to sulfated proteoglycans, while H&E staining provides a broader visualization of tissue structures.

Acute Toxicity of MMOS-Ica@HA to Zebrafish Embryos and Larvae

At 6 hours post-fertilization (hpf), zebrafish embryos were transferred to a 96-well plate and cultured in egg water (100 mL per well). The embryos were then treated with different concentrations of MMOS-Ica@HA (0.25, 0.50, 1.0, 2.0, 5.0, 10, and 20 mg/mL) and placed in an incubator at 28.5 °C. To assess the effects of the treatment, the percent survival and percent of malformed zebrafish were evaluated every 24 h from 24 to 168 hpf using a dissecting microscope. Dead larvae were identified by the absence of cardiac function, lack of response to touch, or decomposition. Malformed larvae were characterized by pericardial edema, axis curvature, yolk sac edema, and cranial and facial abnormalities. The numbers of dead and malformed zebrafish were recorded every 24 h throughout the experiment.

In addition, to measure the antioxidant enzyme activities and oxidative stress markers, specific assay kits were used. Superoxide dismutase (SOD) activity, catalase (CAT) activity, and malondialdehyde (MDA) content were determined using their respective assay kits (Shanghai Enzyme-linked Biotechnology Co., Ltd.). These kits provide standardized protocols and reagents for accurate measurement of SOD and CAT activities, as well as MDA levels.

Statistical Analysis

The experimental data are presented as mean ± S.D. The experiments were performed at least in triplicate, and data were analyzed with the SPSS software using one-way ANOVA followed by a post hoc Tukey's test. The significance level was fixed as $*P < 0.05$, $**P < 0.01$, or $***P < 0.001$.

Results and Discussion

Construction and Characterizations of Nanoplatforms

First, the MON was prepared through a sol-gel approach and then modified with MPTMS to obtain MOS. After that, the Mg-engineered MOS (eg, MMOS) was fabricated a hydrothermal method by using monodispersed MON as a hard template and $MgCl_2$ as a magnesium source. During the hydrothermal process, the reaction between Mg^{2+} and the released silicon-containing oligomers (dissolution process) leads to the formation of a Mg-doped silica layer on the surface of MOS (growth process). This approach is known as the "dissolution-growth" strategy for producing MMOS nanoparticles. Additionally, a similar procedure has been reported for the preparation of biodegradable mesoporous copper silicate nanospheres.[34] As an ideal drug delivery carrier, the Ica was then loaded into MMOS within mesoporous channels to generate MMOS-Ica, and the HA molecules serve as "gatekeepers" for controlling drug release and are further modified on the surface of MOS, resulting in MMOS-Ica@HA. The Ica loading content of MMOS-Ica@HA is determined to be 11.2 ± 0.7% based on the UV-vis analysis, which is higher than previously reported drug delivery systems (around 8.9%).[35]

Figure 1A–C shows the morphology of synthesized MOS, MMOS, and MMOS-Ica@HA, revealing the good aqueous dispersion and spherical capsule morphology of obtained nanoparticles. The prominent spherical nanoplatforms of MMOS-Ica@HA with excellent monodispersity were also confirmed by the SEM observations (Figure 1D). Elemental mapping of MMOS-Ica@HA (Figure 1E) displays a clear presence of N, C, O, Si, S, and Mg, demonstrating the successful formation of the spherical nanoplatform structures and incorporation of Mg ions. Meanwhile, the Mg content in the MMOS-Ica@HA specimen was quantified as 7.8 ± 0.6% by inductively coupled plasma optical emission spectrometry (ICP-OES) test using the Thermo Fisher Scientific iCAP 6300Duo instrument, and the corresponding ratio of Si/Mg is determined to be 6.7.

According to the dynamic light scattering (DLS) analysis, the average particle size of MOS or MMOS is approximately 113 nm or 121 nm, respectively. However, after the conjugation of HA, the particle size slightly increased to around 137 nm (Figure 1F–H). Both the EDX spectrum (Figure 1I) and full-range survey XPS spectrum (Figure 1J) exhibit the homogeneous distributions of N, C, O, Si, S, and Mg signals in MMOS-Ica@HA specimens. The above results all indicate the successful construction of MMOS-Ica@HA nanoplatforms.

Next, the N_2 adsorption isotherm measurements were conducted to determine the specific surface area and average pore size of MOS or MMOS-Ica@HA using the Brunauer-Emmett-Teller (BET) technique. The specific surface area and pore diameter of MOS are determined to be 376.1 $m^2\ g^{-1}$ (Figure S1) and 5.0 nm (Figure 1K), respectively, indicating its ability to provide an appreciable drug encapsulation capacity. After drug loading and modification, the BET area and pore size decreased to 158.9 $m^2\ g^{-1}$ and 4.2 nm, respectively. Figure S2 illustrates the positive colloidal stability of MMOS-Ica@HA in various physiological solutions, such as deionized water, PBS buffer, or DMEM medium. The results of the polydispersity index (PDI) values of MMOS-Ica@HA after 7 days of storage in different media are all less than 0.3 (Figure S3), further demonstrating the favorable dispersibility of our nanoplatforms.

In vitro Biodegradation Behavior and Endocytosis Performance

It is well recognized that MOS frameworks can degrade in response to reducing environments. To validate this hypothesis, TEM images of MMOS-Ica@HA were captured at various incubation time intervals in a simulated body fluid (SBF) solution containing 1.0 mM GSH (Figure 2A). During a 7-day incubation period, the presence of GSH leads to a gradual deformation, collapse, and fragmentation of MMOS-Ica@HA, indicating its biodegradable nature. The degraded 7-day MMOS also shows a similar behavior with visible framework collapse and deformation, while the MOS presents a relatively complete spherical framework (Figure S4), indicating its degradation rate is lower than MMOS or

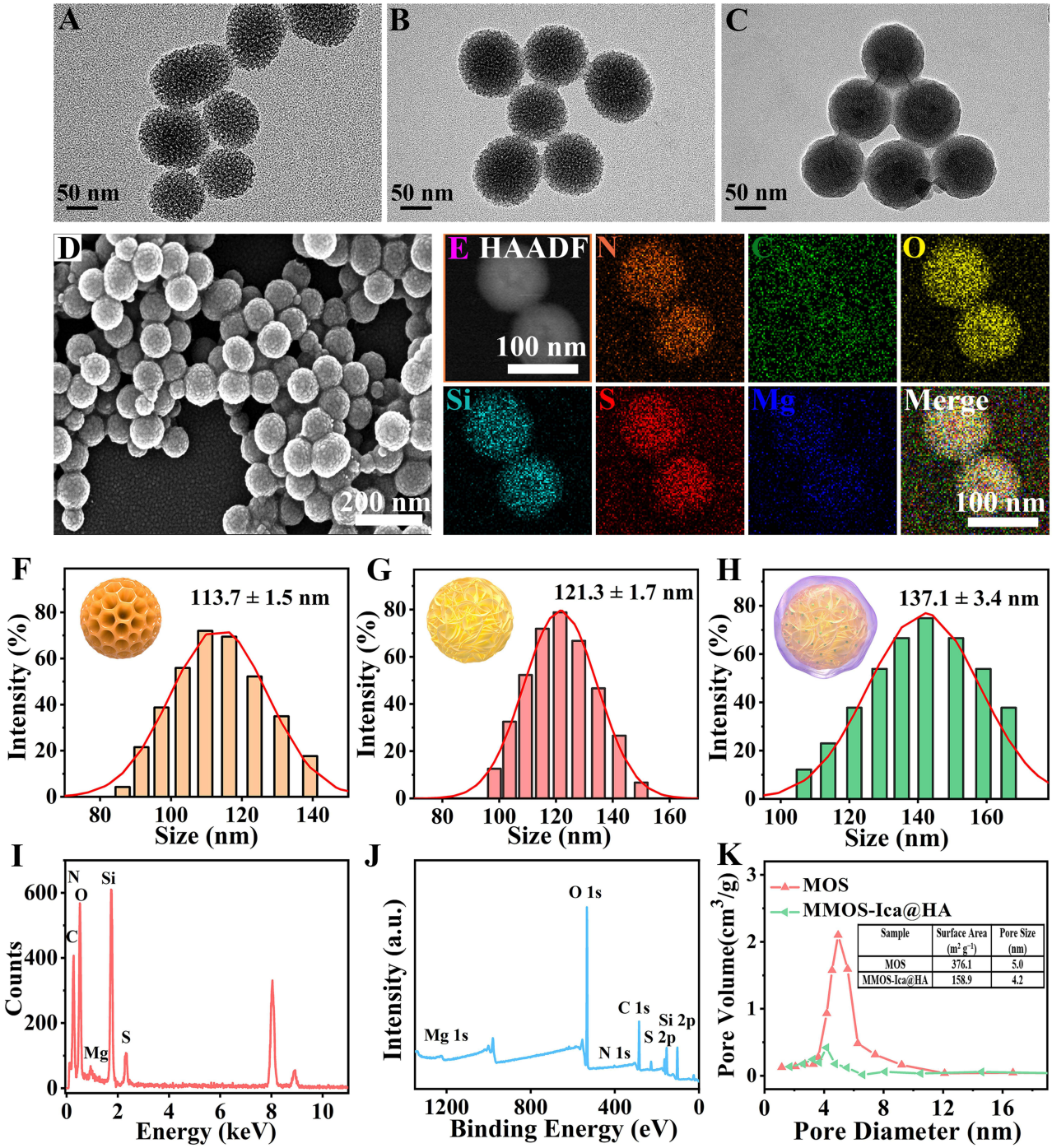

Figure 1 (**A**–**C**) TEM images of MOS (**A**), MMOS (**B**), or MMOS-Ica@HA (**C**). (**D** and **E**) SEM images (**D**) or HAADF-STEM images (**E**) of MMOS-Ica@HA nanoplatforms. (**F**–**H**) Size determination of MOS (**F**), MMOS (**G**), or MMOS-Ica@HA (**H**) via DLS measurements. (**I** and **J**) EDX spectrum (**I**) or full-range survey XPS spectrum (**J**) of MMOS-Ica@HA. (**K**) Pore diameter distribution of MOS or MMOS-Ica@HA.

MMOS-Ica@HA specimen. This is probably because the Mg-engineered process leads to a looser nanoparticle framework, which in turn can further promote nanoparticle degradation in response to reduced GSH, and similar findings have been reported in previous studies.[36]

Building upon the promising outcomes mentioned above, the release of drugs from nanoplatforms in response to stimuli was investigated under various conditions (Figure 2B and C). Due to the presence of disulfide bonds within the MMOS framework, which are highly sensitive to GSH (glutathione), the decomposition of the framework can result in the

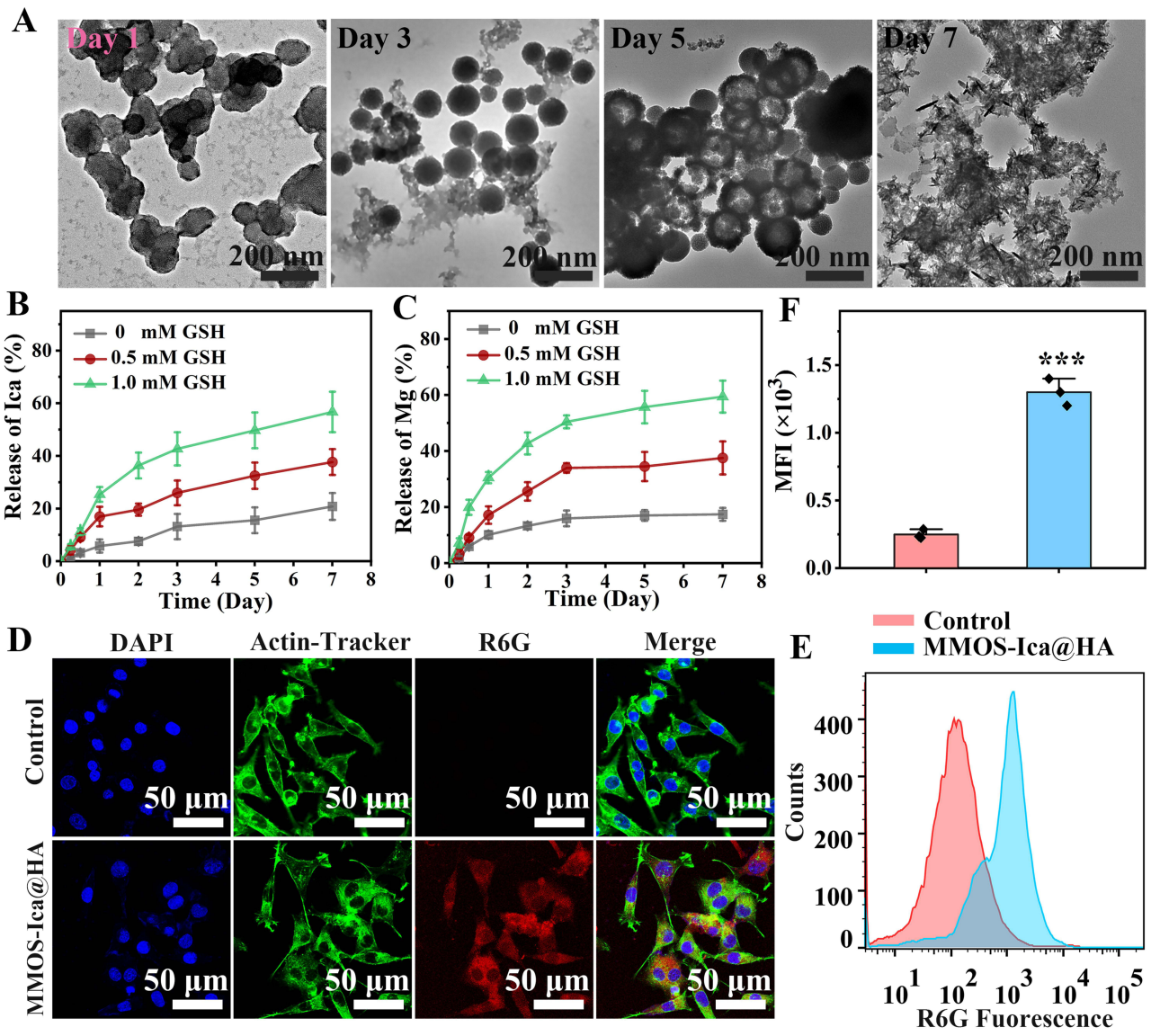

Figure 2 (**A**) TEM images of biodegradable MMOS-Ica@HA after incubation in SBF solution containing 1.0 mM of GSH for 1.0–7.0 days. (**B** and **C**) Release profile of Ica (**B**) or Mg^{2+} (**C**) from nanoplatforms in PBS solution containing GSH. (**D**) CLSM results of BMSCs after treatment with R6G-labelled MMOS-Ica@HA. (**E** and **F**) Flow cytometric analysis on the intracellular R6G fluorescence for BMSCs treated with R6G-labelled MMOS-Ica@HA for 2.0 h. ***$P < 0.001$, represents an extremely significant difference.

detachment of the HA coating layer from MMOS-Ica@HA. This detachment "turns on" the switch of the mesopores, leading to the release of Ica. Simultaneously, as the disulfide bonds are cleared in response to GSH stimulation, the framework is significantly disrupted, further allowing for the controllable release of loaded Ica or Mg components. As expected, the cumulative release of Mg^{2+} or Ica in SBF solution for 7.0 days is only about 20%, while their corresponding cumulative release exceeds 50% under SBF solution with 1.0 mM GSH. Additionally, due to the protection provided by HA "gatekeepers", the MMOS-Ica@HA group exhibits a more stable and sustained release performance compared to the MMOS-Ica sample, which shows relatively rapid burst release behavior upon stimulation by GSH (Figure S5). Notably, the reductive GSH levels can lead to the controlled release of loaded drugs from MMOS-Ica@HA nanoplatforms.

The intracellular endocytosis performance of R6G-labelled MMOS-Ica@HA was evaluated in vitro using both CLSM and flow cytometry techniques. Compared to the control group, CLSM observation displays a significant red fluorescence signal within the cytoplasm for the MMOS-Ica@HA group (Figure 2D). Meanwhile, the positive cellular endocytosis results of the MOS or MMOS treated group are also presented in Figure S6, which reveals the appreciable cellular uptake

capacity of our nanoplatforms based on the enhanced permeability and retention (EPR) effect.[37] The further flow cytometry analysis of the fluorescence intensity of BMSCs also confirms the above conclusion. It can be found that the fluorescence intensity of BMSCs treated with R6G-labelled MMOS-Ica@HA is evidently higher than PBS treated group (Figure 2E and F). The results above suggest the prominent intracellular endocytosis capability of the prepared nanoplatforms.

Biocompatibility Assessment of Nanoplatforms

In vitro cytotoxicity of the resultant nanoplatforms on BMSCs was further examined. Figure 3A and C depict the calcein AM- and propidium iodide (PI) co-stained BMSCs, along with the corresponding quantitative analysis results, following

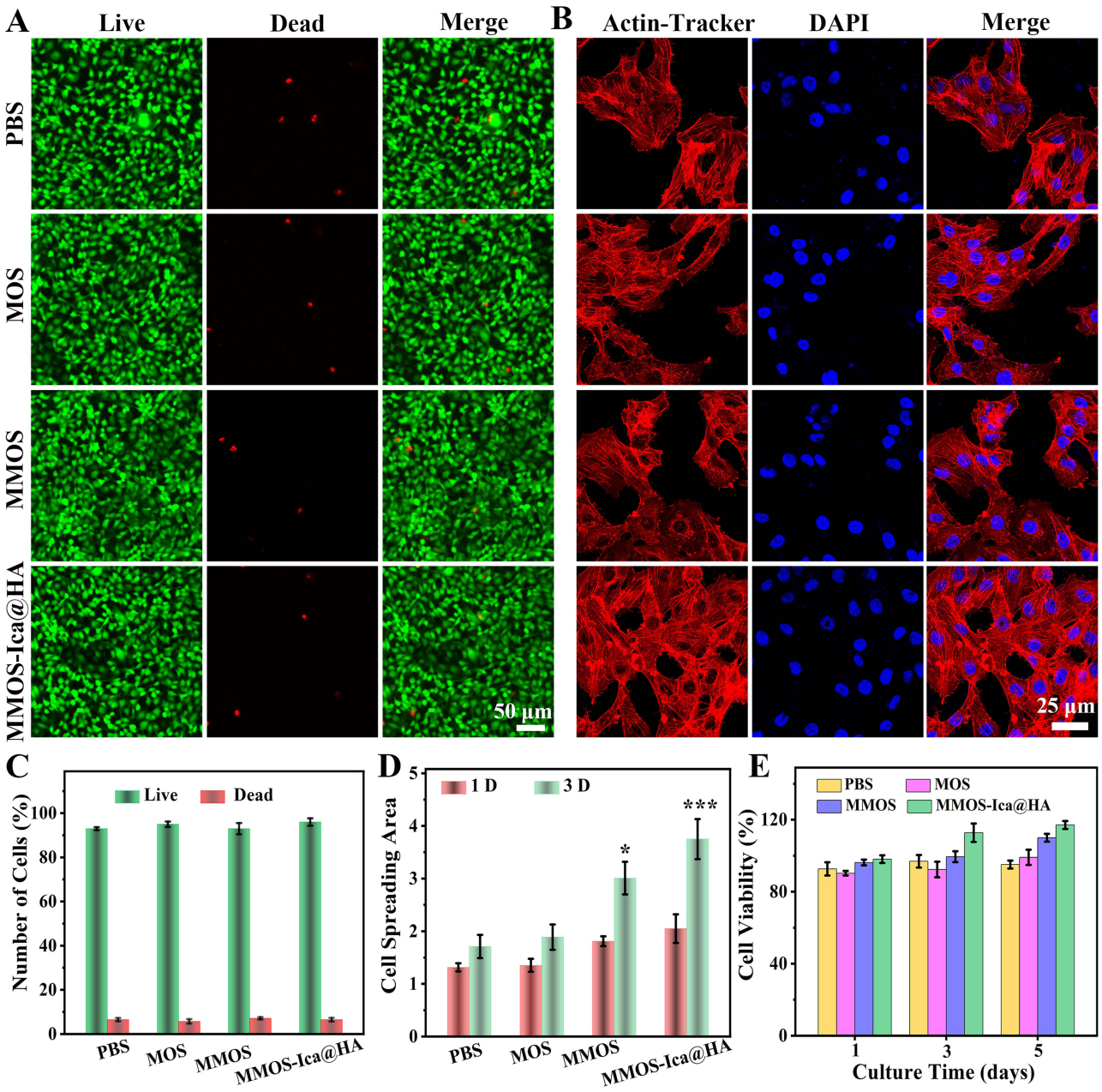

Figure 3 (**A**) Live/dead cell staining of BMSCs cultured with complete culture medium containing PBS, MOS, MMOS, or MMOS-Ica@HA, and (**C**) its quantitative analysis of live/dead cells on day 3.0. (**B**) CLSM images of stained BMSCs visualizing cell morphology after incubation with different formations, and (**D**) its quantitative results of spread area via the Image J software. (**E**) Viability of BMSCs incubated with PBS, MOS, MMOS, or MMOS-Ica@HA for 1.0, 3.0, or 5.0 days. *$P < 0.05$, represents a significant difference. ***$P < 0.001$, represents an extremely significant difference.

incubation with PBS, MOS, MMOS, or MMOS-Ica@HA for 3.0 days. Almost a few dead cells can be found in each treatment group, indicating the favorable biocompatibility of the nanoplatform system. Due to the "gatekeeper" role of HA in providing controlled release of Ica, the cell viability of BMSCs after treatment with MMOS-Ica@HA remains at 99.3% even at high doses of Ica drug (44.8 μg/mL). In contrast, the negative impact of freely diffused Ica on BMSCs is evident in the MMOS-Ica group, where the corresponding cell viability decreases to 85.4% (Figure S7). This decrease is significantly lower than that observed in the MMOS-Ica@HA group under the same conditions ($P < 0.05$). The live/dead staining results of BMSCs after treatment with MMOS-Ica also present a similar trend owing to the sudden release of Ica accompanied by certain cellular side effects (Figure S8). These findings can be consistent with the results of in vitro release, further demonstrating the "gatekeeper" role of HA to optimize drug delivery and decrease the negative impact of rapid drug release on cell viability.

In addition, the analysis of cell morphology (Figure 3B and D) demonstrates that BMSCs incubated with MMOS or MMOS-Ica@HA exhibit a significantly larger spreading area compared to the PBS or MOS group. Especially, BMSCs treated with MMOS-Ica@HA show the largest spreading area and typical slender fusiform shapes with distinct pseudopodia. Previous studies have indicated that moderate levels of Mg^{2+} can not only promote the proliferation and differentiation of chondrocytes but also inhibit their apoptosis.[38–40] Meanwhile, the released Ica from MMOS-Ica@HA also can further combinedly promote the proliferation of BMSCs.[41] Similar findings with positive cell proliferation can be observed in the MTT assays. As depicted in Figure 3E, the BMSCs treated with MMOS-Ica@HA show the highest cell viability compared to other treated groups, proving the existence of Ica and Mg^{2+} have a promoting effect on BMSCs proliferation to a certain extent.

Improvement of Cartilage Differentiation Potential

To examine the impact of nanomedicine on the chondrogenic differentiation behavior of BMSCs, a series of experimental techniques were employed. Immunofluorescence staining, Safranin O, and Alcian staining, as well as RT-qPCR analysis, were performed following a 14-day induction of chondrogenic differentiation. Immunofluorescence staining of SOX9 and Col-II (Figure 4A) reveals that the introduction of the Mg component leads to increased expression of SOX9 and deposition of Col-II compared to the PBS group. Notably, the MMOS-Ica@HA treated group exhibits the highest fluorescence signal, indicating superior cartilage differentiation performance attributed to the combined effects of Ica and Mg. Both Safranin O (Figure 4B) and Alcian (Figure 4C) staining demonstrate successful directed chondrogenic differentiation of BMSCs in the MMOS-Ica@HA treated group in the presence of Mg and Ica. This was evidenced by the abundant production of glycosaminoglycans (GAGs) and the distinct blue staining of mucopolysaccharides in chondrocytes, in contrast to the observations in the PBS or MOS group.

For further assessment of chondrogenic differentiation of BMSCs, the expression levels of chondrogenic markers, including SOX9, ACAN, and Col-II, were quantified using qRT-PCR (Figure 4D–F). The results demonstrated that the MOS groups exhibit a slight enhancement in the expression of chondrogenic genes, while the MMOS group shows partial upregulation. In contrast, the MMOS-Ica@HA group displays a significant improvement in gene expression compared to the PBS group. Evidently, the combined effect of Mg and Ica plays a crucial role in promoting the chondrogenic differentiation of BMSCs. On one hand, the sustained release of Ica positively influenced chondrocyte proliferation and the secretion of proteoglycan and collagen matrix.[42–44] On the other hand, the Mg^{2+} could potentiate the synthesis of the cartilage matrix by activation of the HIF-α pathway,[28,40] as confirmed by Figure 4G, thereby conferring a Mg^{2+}-mediated improvement of cellular chondrogenic regulation. These findings suggest that both Mg and Ica combinedly contribute to the promotion of chondrogenic differentiation in BMSCs, whereas further studies are needed to investigate the cooperative impact of Mg and Ica on chondrogenic differentiation.

In vivo Evaluation of Cartilage Regeneration

Zebrafish chondrodysplasia models were constructed with prednisolone and used to evaluate the potential of cartilage differentiation and regeneration. The morphological findings of Alcian blue staining, together with H&E staining on

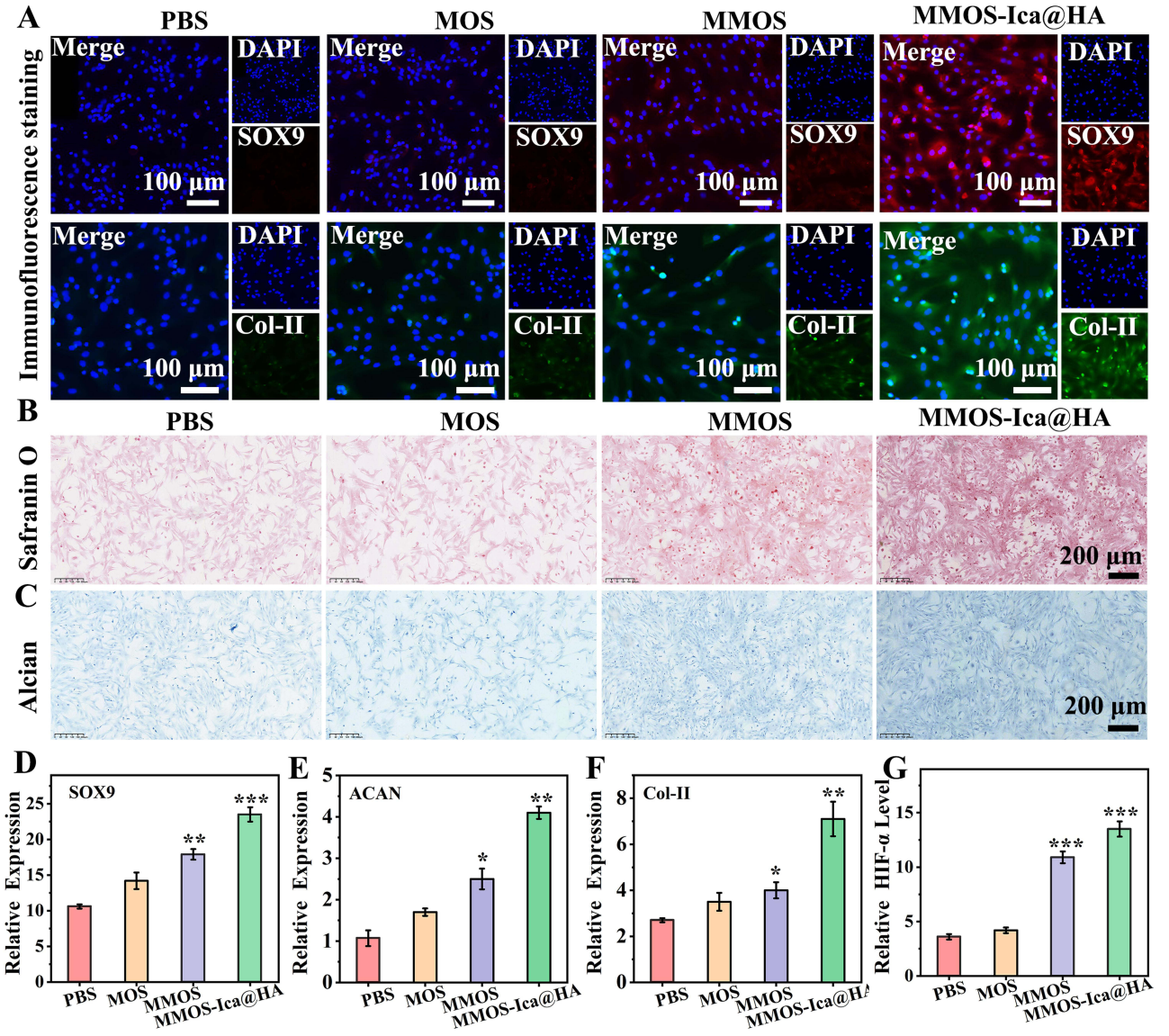

Figure 4 (**A**) Immunofluorescence staining for SOX9 and Col-II expressed in BMSCs incubated with different formulations for 14 days. (**B** and **C**) Safranin O and Alcian staining of the BMSCs after treatment with PBS, MOS, MMOS, or MMOS-Ica@HA. (**D**–**F**) Expression level of chondrogenic-related biomarkers including SOX9, ACAN, and Col-II measured by qRT-PCR assays. (**G**) Quantification of HIF-1α expression level based on the ELISA Kit. *P < 0.05, represents a significant difference. **P < 0.01, represents a very significant difference. ***P < 0.001, represents an extremely significant difference.

craniofacial sections show the effect of nanoplatforms on zebrafish cartilage regeneration. The MMOS-Ica@HA group demonstrated a fully intact distribution of chondrocytes in the craniofacial cartilage structure of zebrafish. Conversely, the cartilage structure of the PBS or MOS treated group exhibited disarray (Figure 5A). As shown in Figure 5B, H&E staining indicated that the chondrocytes of the MMOS-Ica@HA group were oval and deeply stained compared to those of the control group. Furthermore, as the exposure time increased, the demarcation between the ceratohyal chondrocytes became distinct, leading to the gradual growth of the entire craniofacial cartilage. Additionally, the connective tissue layer surrounding the perichondrium thickened. Therefore, our findings from the analysis of pathology (including morphological and histopathological evaluations) suggest that MMOS-Ica@HA nanoplatforms exerted a comprehensive impact on chondrogenesis in the craniofacial cartilage of zebrafish offspring. This led to craniofacial regeneration through the proliferation and differentiation of chondrocytes.

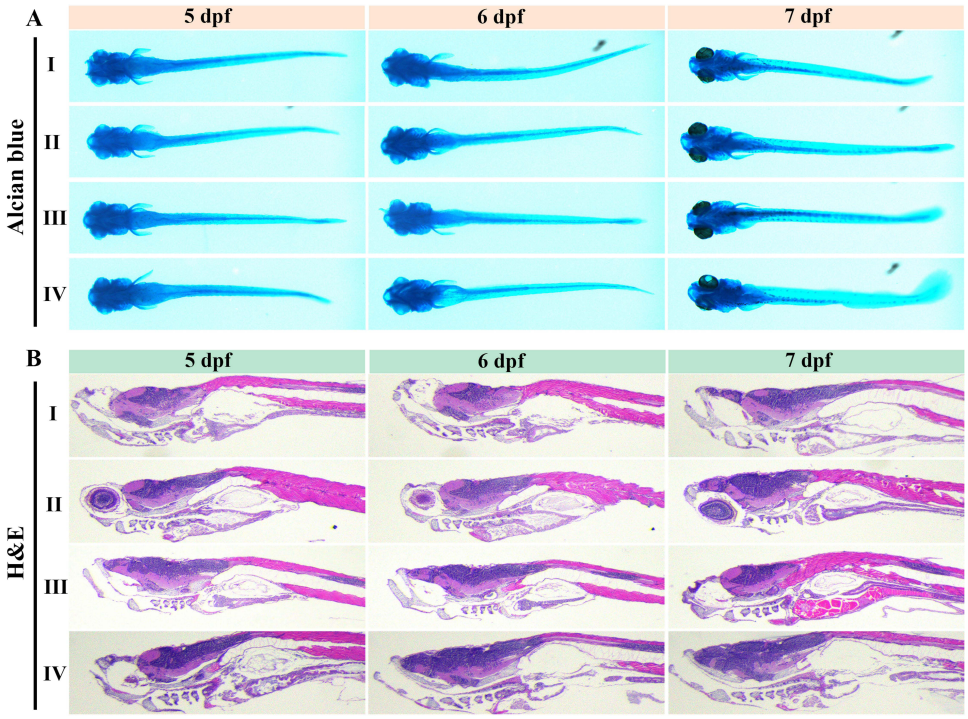

Figure 5 (**A**) Alcian blue and (**B**) H&E staining of zebrafish embryo treated (**I**) PBS, (II) MOS, (III) MMOS, and (IV) MMOS-Ica@HA at 5 dpf, 6 dpf, or 7dpf, showing the craniofacial cartilage regeneration.

Acute Toxicity in Zebrafish Embryo

The acute toxicity of MMOS-Ica@HA at various concentrations (0.25, 0.50, 1.0, 2.0, 5.0, 10, and 20 mg/mL) was assessed on zebrafish embryos or larvae from 1 dpf to 7 dpf. No significant changes are observed in the percent survival of zebrafish embryos and larvae at different developmental stages (1–7 dpf) when exposed to concentrations of MMOS-Ica@HA ranging from 0 to 2.0 mg/mL, while slight toxicity begins to appear at a concentration of 5.0 mg/mL, and over 85% survival rate can be maintained even at concentrations as high as 20 mg/mL (Figures 6A–C and S9). The results clearly demonstrate that MMOS-Ica@HA has minimal impact on the survival of zebrafish and exhibits weak toxicity towards zebrafish. In addition, the percent of malformed zebrafish embryos induced by varying concentrations at 1–7 dpf also validates the prime biosafety performance of the nanoplatform system (Figures 6D–F and S10), the toxic effect of MMOS-Ica@HA at different concentrations (<5.0 mg/mL) on the morphological development of zebrafish is almost negligible.

According to previous studies, it has been shown that the toxicity induced by nanoparticles can trigger oxidative stress reactions, leading to an increase in the production of reactive oxygen species.[45,46] Consequently, we measured the levels of the index (CAT, SOD, and MDA) related to oxidative stress in the pharyngeal arch of zebrafish embryos exposed to MMOS-Ica@HA. Figure 6G–I show the CAT, SOD, and MDA level of zebrafish embryo treated with different concentrations, respectively. There are no significant differences were observed between the MMOS-Ica@HA-treated group with a concentration of 5.0 mg/mL and the normal control group. This suggests that the oxidative stress induced by MMOS-Ica@HA has a negligible or low impact on zebrafish embryos. Hence, it can be inferred that MMOS-Ica@HA nanoplatforms do not exhibit significant toxicity during the developmental stages of zebrafish.

In summary, although the Ica-loaded nanoplatform has shown efficacy in chondrogenesis and chondrocyte proliferation, the reproducibility of results when using it in chondrodysplasia still requires more research. Furthermore, in the present study, the absence of additional evaluation regarding the treatment of chondrodysplasia using MOS-Ica@HA particles hinders a more robust demonstration of the collaborative effect between the Ica and Mg components. In future studies, an in-depth understanding of the different subtypes of chondrodysplasia and the optimization of therapeutic

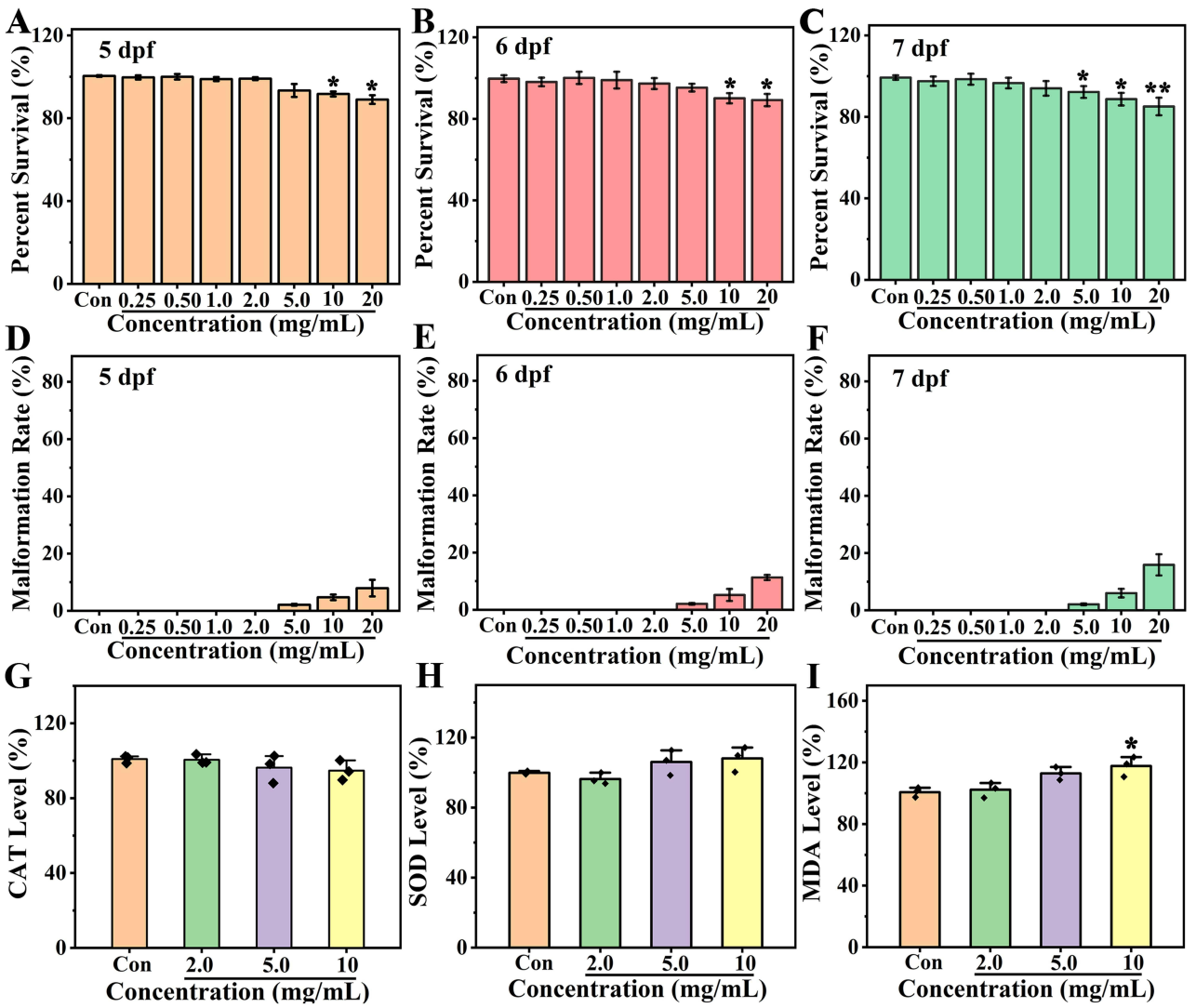

Figure 6 (**A**–**C**) Percent survival of zebrafish embryo treated with various concentrations of MMOS-Ica@HA at 5–7 dpf. (**D**–**F**) Percent of malformed zebrafish embryo at 5–7 dpf. (**G**–**I**) Effect of MMOS-Ica@HA on the oxidative stress level of zebrafish embryos, including MDA, SOD, and CAT. *$P < 0.05$, represents a significant difference. **$P < 0.01$, represents a very significant difference.

parameters for MMOS-Ica@HA, as well as rigorous study design and implementation, will help to assess and ensure the reproducibility of nanomedicine in the treatment of chondrogenesis.

Conclusions

In summary, a biodegradable MMOS-Ica@HA nanoplatform is proposed for chondrodysplasia treatment. The findings of TEM images, particle diameter by DLS, STEM mapping, EDX, XPS, and BET analysis all validate the successful preparation of the MMOS-Ica@HA. Due to its specific degradation behavior, the MMOS-Ica@HA shows controlled drug release with negligible cytotoxicity. In addition, the biocompatible nanoplatforms display superior advantages for inducing BMSCs proliferation and differentiation in vitro owing to the collaborative promotion of released Mg^{2+} and Ica. Further results of in vivo zebrafish embryo with chondrodysplasia shows the prominent performance of cartilage regeneration and excellent biocompatibility. All these results suggest that the MMOS-Ica@HA nanomedicine formulation exhibits a satisfactory effect on cartilage differentiation and reconstruction. This finding provides an alternative and promising strategy to address chondrodysplasia, warranting further investigation to facilitate its potential clinical application.

Acknowledgments

This work was supported by the Guangzhou Science and Technology Program (No. 2021020xxx), the health science and technology project of Guangzhou (No.20231A011092), and the Guangdong Science and Technology Program (No. 2022A1515220043), China.

Disclosure

The authors declare no conflicts of interest in this work.

References

1. Verstraeten A, Meester J, Peeters S, Mortier G, Loeys B. Chondrodysplasias and aneurysmal thoracic aortopathy: an emerging tale of molecular intersection. *Trends Mol Med*. 2020;26(8):783–795. doi:10.1016/j.molmed.2020.05.004
2. Kumar R, Sood A, Marwah A, Sharma R, Padhy AK, Moorthy D. Metaphyseal chondrodysplasia: interesting findings on bone scintigraphy. *Clin Nucl Med*. 2000;25(12):1047–1049.
3. Barna M, Niswander L. Visualization of cartilage formation: insight into cellular properties of skeletal progenitors and chondrodysplasia syndromes. *Dev Cell*. 2007;12(6):931–941.
4. Weir EC, Philbrick WM, Amling M, Neff LA, Baron R, Broadus AE. Targeted overexpression of parathyroid hormone-related peptide in chondrocytes causes chondrodysplasia and delayed endochondral bone formation. *Proc Natl Acad Sci*. 1996;93(19):10240–10245. doi:10.1073/pnas.93.19.10240
5. Heikoop J, Van Roermund C, Just W, et al.; Rhizomelic chondrodysplasia punctata. Deficiency of 3-oxoacyl-coenzyme A thiolase in peroxisomes and impaired processing of the enzyme. *J Clin Invest*. 1990;86(1):126–130. doi:10.1172/JCI114674
6. İli EG, Gezdirici A, Di Pietro E, Yergeau C, Braverman N. Expanding the genotypic and phenotypic landscapes of rhizomelic chondrodysplasia punctata type 3 (RCDP3) with two novel families, and a review of the literature. *Am J Med Genet A*. 2022;188(11):3229–3235. doi:10.1002/ajmg.a.62959
7. Sayed J, Gamal A, Theyab A, Algahtani M, Aldaadi BB. Neonatal rhizomelic chondrodysplasia punctata type 2 caused by a novel homozygous variant in the GNPAT gene. *Clin Case Rep*. 2023;11(6):e7504. doi:10.1002/ccr3.7504
8. Han X, Alu A, Liu H, et al. Biomaterial-assisted biotherapy: a brief review of biomaterials used in drug delivery, vaccine development, gene therapy, and stem cell therapy. *Bioact Mater*. 2022;17:29–48. doi:10.1016/j.bioactmat.2022.01.011
9. Chitranshi N, Rajput R, Godinez A, et al. Neuroserpin gene therapy inhibits retinal ganglion cell apoptosis and promotes functional preservation in glaucoma. *Mol Ther*. 2023;31(7):2056–2076. doi:10.1016/j.ymthe.2023.03.008
10. Mao C, Xiang Y, Liu X, et al. Repeatable photodynamic therapy with triggered signaling pathways of fibroblast cell proliferation and differentiation to promote bacteria-accompanied wound healing. *ACS Nano*. 2018;12(2):1747–1759. doi:10.1021/acsnano.7b08500
11. Xu X, Liang Y, Li X, et al. Exosome-mediated delivery of kartogenin for chondrogenesis of synovial fluid-derived mesenchymal stem cells and cartilage regeneration. *Biomaterials*. 2021;269:120539. doi:10.1016/j.biomaterials.2020.120539
12. Liu Y, Yang J, Luo Z, et al. Development of an injectable thiolated icariin functionalized collagen/hyaluronic hydrogel to promote cartilage formation in vitro and in vivo. *J Mat Chem B*. 2019;7(17):2845–2854. doi:10.1039/C9TB00211A
13. Yang J, Liu Y, He L, et al. Icariin conjugated hyaluronic acid/collagen hydrogel for osteochondral interface restoration. *Acta Biomater*. 2018;74:156–167.
14. Wang ZC, Sun HJ, Li KH, Fu C, Liu MZ. Icariin promotes directed chondrogenic differentiation of bone marrow mesenchymal stem cells but not hypertrophy in vitro. *Exp Ther Med*. 2014;8(5):1528–1534. doi:10.3892/etm.2014.1950
15. Zhang L, Zhang X, K-F L, et al. Icariin promotes extracellular matrix synthesis and gene expression of chondrocytes in vitro. *Phytother Res*. 2012;26(9):1385–1392. doi:10.1002/ptr.3733
16. Ziadlou R, Barbero A, Martin I, et al. Anti-inflammatory and chondroprotective effects of vanillic acid and epimedin C in human osteoarthritic chondrocytes. *Biomolecules*. 2020;10(6):932. doi:10.3390/biom10060932
17. Yao B, Liu J, Xu D, et al. Dissection of the molecular targets and signaling pathways of Guzhi Zengsheng Zhitongwan based on the analysis of serum proteomics. *ChinMed*. 2019;14:1–15.
18. Ohba S, Hojo H, Chung U-I. Bioactive factors for tissue regeneration: state of the art. *Muscles Ligaments Tendons J*. 2012;2(3):193.
19. Lyu Y, Zeng W, Du G, Chen J, Zhou J. Efficient bioconversion of epimedin C to icariin by a glycosidase from Aspergillus nidulans. *Bioresour Technol*. 2019;289:121612. doi:10.1016/j.biortech.2019.121612
20. Huang L, Zhu J, Xiong W, et al. Tumor-generated reactive oxygen species storm for high-performance ferroptosis therapy. *ACS Nano*. 2023;17(12):11492–11506. doi:10.1021/acsnano.3c01369
21. Huang L, Lu Y, Guo S, et al. A strategy of limited-space controlled aggregation for generic enhancement of drug loading capability. *Adv Funct Mater*. 2023;33(4):2209278. doi:10.1002/adfm.202209278
22. Huang L, Feng J, Fan W, et al. Intelligent pore switch of hollow mesoporous organosilica nanoparticles for high contrast magnetic resonance imaging and tumor-specific chemotherapy. *Nano Lett*. 2021;21:9551.
23. Gao F, Wu J, Niu S, et al. Biodegradable, pH-sensitive Hollow Mesoporous Organosilica Nanoparticle (HMON) with Controlled Release of Pirfenidone and Ultrasound-Target-Microbubble-Destruction (UTMD) for pancreatic cancer treatment. *Theranostics*. 2019;9(20):6002. doi:10.7150/thno.36135
24. Hsieh V, Okada S, Wei H, et al. Neurotransmitter-responsive nanosensors for T2-weighted magnetic resonance imaging. *J Am Chem Soc*. 2019;141(40):15751–15754. doi:10.1021/jacs.9b08744
25. Zhao Y, He P, Yao J, et al. pH/NIR-responsive and self-healing coatings with bacteria killing, osteogenesis, and angiogenesis performances on magnesium alloy. *Biomaterials*. 2023;301:122237.

26. Huang L, Li W, Guo M, et al. Silver doped-silica nanoparticles reinforced poly (ethylene glycol) diacrylate/hyaluronic acid hydrogel dressings for synergistically accelerating bacterial-infected wound healing. *Carbohydr Polym*. 2023;304:120450. doi:10.1016/j.carbpol.2022.120450
27. Wang L, Huo M, Chen Y, Shi J. Iron-engineered mesoporous silica nanocatalyst with biodegradable and catalytic framework for tumor-specific therapy. *Biomaterials*. 2018;163:1–13. doi:10.1016/j.biomaterials.2018.02.018
28. Liao Z, Fu L, Li P, et al. Incorporation of magnesium ions into an aptamer-functionalized ECM bioactive scaffold for articular cartilage regeneration. *ACS Appl Mater Interfaces*. 2023;15(19):22944–22958. doi:10.1021/acsami.3c02317
29. Yang J, Zhang X, Chen J, et al. Macrophages promote cartilage regeneration in a time- and phenotype-dependent manner. *J Cell Physiol*. 2022;237 (4):2258–2270. doi:10.1002/jcp.30694
30. Chen Y, Chen Y, Xiong X, et al. Hybridizing gellan/alginate and thixotropic magnesium phosphate-based hydrogel scaffolds for enhanced osteochondral repair. *Mater Today Bio*. 2022;14:100261. doi:10.1016/j.mtbio.2022.100261
31. Yao H, Xu J, Wang J, et al. Combination of magnesium ions and vitamin C alleviates synovitis and osteophyte formation in osteoarthritis of mice. *Bioact Mater*. 2021;6(5):1341–1352. doi:10.1016/j.bioactmat.2020.10.016
32. Gao C, Dai W, Wang X, et al. Magnesium gradient-based hierarchical scaffold for dual-lineage regeneration of osteochondral defect. *Adv Funct Mater*. 2023;33(43):2304829. doi:10.1002/adfm.202304829
33. Pontes Mauricio H, Yeom J, Groisman Eduardo A. Reducing ribosome biosynthesis promotes translation during low Mg2+ stress. *Molecular Cell*. 2016;64(3):480–492. doi:10.1016/j.molcel.2016.05.008
34. Liu C, Wang D, Zhang S, et al. Biodegradable biomimic copper/manganese silicate nanospheres for chemodynamic/photodynamic synergistic therapy with simultaneous glutathione depletion and hypoxia relief. *ACS nano*. 2019;13(4):4267–4277. doi:10.1021/acsnano.8b09387
35. Hadipour Moghaddam SP, Yazdimamaghani M, Ghandehari H. Glutathione-sensitive hollow mesoporous silica nanoparticles for controlled drug delivery. *J Control Release*. 2018;282:62–75. doi:10.1016/j.jconrel.2018.04.032
36. Ma Y, Su Z, Zhou L, et al. Biodegradable metal–organic-framework-gated organosilica for tumor-microenvironment-unlocked glutathione-depletion-enhanced synergistic therapy. *Adv Mater*. 2022;34(12):2107560. doi:10.1002/adma.202107560
37. Huang L, Feng J, Zhu J, et al. A strategy of Fenton reaction cycloacceleration for high-performance ferroptosis therapy initiated by tumor microenvironment remodeling. *Adv Healthcare Mater*;2023. 2203362. doi:10.1002/adhm.202203362
38. Bonifacio MA, Cometa S, Cochis A, et al. A bioprintable gellan gum/lignin hydrogel: a smart and sustainable route for cartilage regeneration. *Int J Biol Macromol*. 2022;216:336–346. doi:10.1016/j.ijbiomac.2022.07.002
39. Yue J, Jin S, Gu S, Sun R, Liang Q. High concentration magnesium inhibits extracellular matrix calcification and protects articular cartilage via Erk/autophagy pathway. *J Cell Physiol*. 2019;234(12):23190–23201. doi:10.1002/jcp.28885
40. Zhao J, Wu H, Wang L, et al. The beneficial potential of magnesium-based scaffolds to promote chondrogenesis through controlled Mg2+ release in eliminating the destructive effect of activated macrophages on chondrocytes. *Biomater Adv*. 2022;134:112719. doi:10.1016/j.msec.2022.112719
41. Tang W, Zhang H, Liu D, Jiao F. Icariin accelerates cartilage defect repair by promoting chondrogenic differentiation of BMSCs under conditions of oxygen-glucose deprivation. *J Cell Mol Med*. 2022;26(1):202–215. doi:10.1111/jcmm.17073
42. Zhang M, Jia G, Weng J, et al. A novel scaffold of icariin/porous magnesium alloy repaired knee cartilage defect in rat by Wnt/β-catenin signaling pathway; 2023.
43. Coaccioli S, Sarzi-Puttini P, Zis P, Rinonapoli G, Varrassi G. Osteoarthritis: new insight on its pathophysiology. *J Clin Med*. 2022;11(20):6013. doi:10.3390/jcm11206013
44. Chen M, Lu L, Cheng D, et al. Icariin promotes osteogenic differentiation in a cell model with NF1 gene knockout by activating the cAMP/PKA/CREB pathway. *Molecules*. 2023;28(13):5128. doi:10.3390/molecules28135128
45. Hussain SM, Javorina AK, Schrand AM, Duhart HM, Ali SF, Schlager JJ. The interaction of manganese nanoparticles with PC-12 cells induces dopamine depletion. *Toxicol Sci*. 2006;92(2):456–463. doi:10.1093/toxsci/kfl020
46. Li N, Sioutas C, Cho A, et al. Ultrafine particulate pollutants induce oxidative stress and mitochondrial damage. *Environ Health Perspect*. 2003;111 (4):455–460. doi:10.1289/ehp.6000